Yun, X. and Gardner, L. (2018) Numerical modelling and design of hot-rolled and cold-formed steel continuous beams with tubular cross-sections. Thin-walled Structures, 132, 574-584.

Numerical modelling and design of hot-rolled and cold-formed steel continuous beams with tubular cross-sections

Xiang Yun*, Leroy Gardner

Department of Civil and Environmental Engineering, Imperial College London, London, UK

*Corresponding author. E-mail address: x.yun14@imperial.ac.uk

Abstract: The structural behaviour and design of hot-rolled and cold-formed steel continuous beams with square and rectangular hollow sections are studied in the present paper, with a focus on the beneficial effects of material strain hardening and moment redistribution. Finite element (FE) models were first developed and validated against existing test results on hot-rolled and cold-formed steel square and rectangular hollow section continuous beams. Upon validation against the experimental results, parametric studies were carried out to expand the available structural performance data over a range of cross-section geometries, cross-section slendernesses, steel grades and loading conditions. Representative material properties and residual stress patterns were incorporated into the FE models to reflect the two studied production routes – hot-rolling and cold-forming. The experimental results, together with the parametric numerical results generated herein, were then used to evaluate the accuracy of the design provisions of EN 1993-1-1 [1] as well as the continuous strength method (CSM) for indeterminate structures, the latter of which is extended in scope in the present study. It was shown that the current provisions of EN 1993-1-1 [1] for the design of hot-rolled and cold-formed steel continuous beams are rather conservative, while the proposed CSM yields a higher level of accuracy and consistency, due to its rational consideration of both strain hardening at

the cross-sectional level and moment redistribution at the global system level. Finally, statistical analyses were carried out to assess the reliability level of the two design methods according to EN 1990 (2002).

Keywords: Cold-formed steel; Continuous beams; Continuous strength method; Hot-rolled steel; Indeterminate structures; Numerical modelling; Parametric study; Plastic design; Reliability analysis; Rotation capacity; Tubular sections.

1. Introduction

Square and rectangular hollow sections (SHS and RHS, respectively) are widely used across a range of applications within the construction industry, owing principally to their favourable structural properties, inherent aesthetic advantages and ease of prefabrication and mass production. These sections are manufactured following one of two main production routes: hot-rolling and cold-forming. Hot-rolled hollow sections are produced or finished at temperatures above the recrystallization temperature, while cold-formed hollow sections are manufactured at room temperature and undergo significant plastic deformation during the fabrication process. The different production routes lead to significant differences in both the material stress-strain characteristics and residual stresses that arise in the final cross-sections. Hot-rolled steel sections typically exhibit linear elastic material behaviour up to the yield stress and a yield plateau before strain hardening is encountered [2], while cold-formed steel sections have a more rounded stress-strain response with an increased yield strength over the unformed material, but reduced ductility [3]. Residual stresses in hot-rolled hollow sections are generally of low magnitude due to the relatively uniform cooling associated with the regular geometry and constant thickness of tubular sections. For cold-formed hollow sections, the formation of residual stresses is largely associated with non-uniform plastic deformation during the section

production process, causing predominantly through-thickness bending residual stresses around the cross-section. Detailed information on the mechanical properties, residual stress distributions and structural performance of hot-rolled and cold-formed SHS and RHS can be found in [4-8].

For cross-section design, hot-rolled and cold-formed SHS and RHS are generally treated in the same manner in existing steel design specifications (e.g. EN 1993-1-1 [1] and AISC 360-16 [9]) using an elastic-perfectly plastic material model, without considering the differences in their material properties. The current design codes adopt the concept of cross-section classification, and classify cross-sections into discrete behavioural classes based upon the susceptibility of the most slender plate element in the cross-section to local buckling. For the design of indeterminate steel structures, the European code EN 1993-1-1 [1] considers moment redistribution by allowing plastic design to be used for structures with Class 1 cross-sections, which are assumed to have sufficient rotation capacity required from plastic analysis without reduction of their resistances, but plastic design is not currently permitted for structures with higher cross-section classes. The existing design approaches are often found to be conservative in estimating the cross-section resistances of stocky hot-rolled and cold-formed steel SHS and RHS [4,10-14], due to the neglect of the beneficial strain hardening effect, and also create discontinuous steps in the capacity predictions of indeterminate structures at boundaries between different classes, owing to the limitations of the conventional classification system (e.g. limiting the cross-section bending resistance to the plastic moment capacity M_{pl} for Class 1 or Class 2 sections and the elastic moment capacity M_{el} for Class 3 sections, and allowing full moment redistribution for structures with Class 1 sections but no moment redistribution for structures with higher class sections). It is therefore considered necessary to develop more efficient and accurate design approaches for indeterminate structures that can rationally

account for strain hardening effects at the cross-sectional level and moment redistribution at the global system level.

The continuous strength method (CSM) is a deformation based design approach that provides an alternative treatment to cross-section classification and enables the effective exploitation of strain hardening [15]. The CSM has recently been extended to the design of stainless steel and aluminium alloy continuous beams [16-19], and shown to provide more accurate and consistent capacity predictions. The purpose of the present paper is to investigate the feasibility of applying the CSM to hot-rolled and cold-formed steel continuous beams, based on the recent CSM proposals for hot-rolled and cold-formed steel cross-sections under isolated loading (i.e. pure compression and pure bending) [11,12]. Finite element (FE) models, considering the different characteristics (i.e. material stress-strain properties and residual stress patterns) of hot-rolled and cold-formed steel sections, were first developed and validated against the results of the hot-rolled and cold-formed steel continuous beam tests conducted by Gardner et al. [4]. Secondly, an extensive parametric study was carried out to generate additional structural performance data for hot-rolled and cold-formed steel continuous beams with a range of cross-section geometries, cross-section slendernesses, steel grades and loading conditions. The design provisions of EN 1993-1-1 [1] and the proposed CSM for indeterminate structures were then assessed based on the results of the parametric study, together with the collected experimental data. Finally, the applicability and reliability of the proposed CSM for hot-rolled and cold-formed steel continuous beams are evaluated by means of statistical analyses.

2. Summary of previous experimental investigation

The experimental investigation conducted by Gardner et al. [4], which reported a total of 12 test results on hot-rolled and cold-formed steel continuous beams with square and rectangular

hollow sections (SHS and RHS, respectively), is summarized in this section and used for validation of the finite element (FE) model and the assessment of design proposals in Sections 3 to 5. The experimental programme consisted of 12 continuous beam tests on specimens with three different nominal cross-section sizes; for each cross-section size, two hot-rolled and two cold-formed specimens were tested. Table 1 summarizes the measured geometric properties of the test specimens using the symbols illustrated in Fig. 1, where H is the height of the section, B is the width of the section, t is the thickness of the section, r_i is the inner corner radius and $h = H - 2t - 2r_i$ and $b = B - 2t - 2r_i$ are the flat width of flange and web, respectively. In Table 1, the specimens are labelled according to their cross-sectional shape, cross-sectional dimensions, production routes and specimen number. For example, the label RHS 60×40×4 HR1 defines an RHS with nominal cross-sectional dimensions of height H (60 mm) × width B (40 mm) × thickness t (4 mm), and it is the first of the two hot-rolled (HR) test specimens. Note that the letters "CF" in the labels indicate a cold-formed specimen.

The material properties of the investigated hot-rolled and cold-formed sections were determined by tensile coupon tests. Flat coupons were taken from the centre of the face opposite to the weld in the longitudinal direction of all specimens. For the cold-formed sections, corner coupons were also extracted and tested in order to characterize the material properties in the corner regions, where strength enhancements arise due to the large plastic deformations experienced during the manufacturing process. A summary of the measured tensile material properties for each cross-section size is given in Table 2, where E is the Young's modulus, f_y is the material yield strength (taken as the 0.2% proof stress for the cold-formed steel), f_u is the ultimate tensile strength and ε_f is the strain at fracture measured over the standard gauge length. As expected, a sharply defined yield point, followed by a yield plateau and a moderate degree

of strain hardening, was observed in the hot-rolled steel coupon tests, while a rounded stress-strain response with no sharply defined yield point was observed for the cold-formed material.

The beam specimens were 2400 mm in length and were continuously supported over two equal spans of 1100 mm each (i.e. equal to L_1 + L_2), as shown in Fig. 2. The loads were applied symmetrically at two points through steel loading plates within the span, using a spreader beam (see Fig. 2). According to the position of the applied loads along the continuous beam specimens, two five-point bending test configurations were employed in the experimental programme. The first five-point bending configuration is designated "1/3 Span" in Table 1, where the concentrated loads were applied at a distance of one-third of the span from the centre support (i.e. L_1 = 733.3 mm and L_2 = 336.7 mm), while in the second configuration, designated "1/2 Span" in Table 1, the continuous beams were subjected to concentrated mid-span loads (i.e. L_1 = L_2 = 550 mm). The different loading conditions were adopted in order to evaluate the influence of moment gradient, sequence of hinge formation and different plastic hinge rotation demands, on the performance of hot-rolled and cold-formed steel continuous beams. Steel rollers were employed beneath steel loading plates to allow free rotation about the axis of bending at the beam ends and central support, and wooden blocks were inserted into the tubular specimens at the loading points and central support to prevent web crippling due to the localised point loading. The applied load, vertical displacement at the loading points and rotations at the beam ends and central support were measured and detailed in Gardner et al. [4].

3. Numerical investigation

A numerical modelling study of hot-rolled and cold-formed steel SHS and RHS continuous beams was also conducted, using the nonlinear FE analysis package ABAQUS [20]. The results of the 12 continuous beam tests summarized in the previous section were initially used to

validate the developed FE models, which were subsequently employed in a comprehensive parametric study to expand the available experimental database over a wider range of cross-section geometries, cross-section slendernesses, steel grades and loading configurations. Finally, the data generated through the parametric study together with the experimental results were used to evaluate the accuracy of existing and proposed design approaches for continuous beams.

3.1. Modelling assumptions

The four-noded doubly curved shell element with reduced integration and finite membrane strains, designated S4R [20], was selected as the element type in the present study, which has been successfully employed in previous numerical studies on hot-rolled and cold-formed steel tubular sections [11,12]. A mesh convergence study was carried out to obtain an optimum mesh size which provides reliable FE results at reasonable computational costs. Consequently, an element size equal to one twentieth of the width of the most slender plate (i.e. the maximum value of 1/20h and 1/20b) was adopted for the flat portions of the modelled specimens, while, in order to accurately capture the curved corner geometry of the SHS and RHS, a finer mesh of four elements was used in the corner regions. Since the geometry, boundary conditions and loading employed in the test set-up were symmetric with respect to the plane at the central support, and the observed failure modes were symmetric, only one half of the beam length was modelled, with suitable symmetry boundary conditions applied. The load-deformation histories and failure modes from the full model and the half model were found to match precisely, while the half model saved a significant amount of computational time and therefore adopted in the present study.

The engineering stress-strain curves obtained from the tensile coupon tests were first converted into the form of true stress σ_{true} and logarithmic plastic strain $\varepsilon_{ln,pl}$ using Eqs. (1) and (2), where E is the Young's modulus, and σ_{nom} and ε_{nom} are the engineering (nominal) stress and strain, respectively, before being incorporated into the FE models.

$$\sigma_{true} = \sigma_{nom}(1+\varepsilon_{nom}) \tag{1}$$

$$\varepsilon_{ln,pl} = \ln(1+\varepsilon_{nom}) - \frac{\sigma_{nom}}{E} \tag{2}$$

As previously mentioned, non-homogeneity of material properties is often observed in cold-formed sections due to the different levels of cold-working experienced at different locations around the section shape; the corner regions of cold-formed sections experience high levels of plastic deformation and thus exhibit a significant increase in both the yield strength and the ultimate strength, but a corresponding loss in ductility. According to the findings of previous experimental research [21,22], the effect of corner strength enhancement is not limited to the corner regions, but also extends into the adjacent flat portions beyond the corners to a certain distance. This effect was considered in the FE models and a sensitivity study was conducted to investigate the extent to which corner strength enhancement continues beyond the corner regions in the case of cold-formed steel SHS and RHS. In the FE sensitivity study, the measured corner material properties were assigned to three different regions: (1) the corner regions only, (2) the corner regions plus adjacent flat portions extending beyond the corners to a distance of t (where t is the material thickness) and (3) the corner regions plus adjacent flat portions extending beyond the corners to a distance of 2t; the material properties obtained from the cold-formed steel flat tensile coupons were assigned to the remaining regions of the FE models.

With regards to the hot-rolled steel SHS and RHS which generally have homogeneous material properties, the measured stress-strain curves from the flat tensile coupon tests were incorporated into the FE models and assigned to the entire cross-section.

For hot-rolled steel sections, residual stresses are introduced primarily due to the non-uniform cooling rates that arise during fabrication, with the more rapidly cooling regions of the sections being left in residual compression and the slower cooling regions in residual tension. Longitudinal membrane residual stresses are typically dominant over bending residual stresses in hot-rolled steel sections, and thus only membrane residual stresses were considered in the FE models developed herein. The membrane residual stress distribution for hot-rolled steel SHS and RHS, recommended by the European Convention for Constructional Steelwork (ECCS) [23], is shown in Fig. 3(a), where compressive residual stresses are designated as positive and tensile residual stresses as negative. The magnitude of the residual stresses relates to a reference yield stress $\overline{f_{\mathrm{y}}} = 235$ MPa [24]. To simplify the ECCS residual stress distribution for ease of application in FE modelling, a modified residual stress pattern was proposed by Nseir [8], as indicated in Fig. 3(b). In the simplified residual stress pattern, a constant magnitude of $0.5\overline{f_{\mathrm{y}}}$ was assumed for the compressive residual stresses in the corner regions while the amplitude of the tensile residual stresses in the flat regions were determined to achieve self-equilibrium. This simplified residual stress pattern was introduced into the numerical models of the hot-rolled SHS and RHS developed herein for both validation and parametric analyses. For the cold-formed steel SHS and RHS, residual stresses were not explicitly incorporated into the FE models for two reasons: (1) the dominant longitudinal bending residual stresses are, to a large extent, inherently incorporated into the stress-strain curves obtained from tensile coupon tests [25], and (2) the membrane residual stresses have

been shown to be negligible and have little influence on the behaviour of cold-formed steel SHS and RHS [4,8].

Owing to the absence of global buckling, only local geometric imperfections were considered in the FE models. An elastic buckling analysis was first carried out for each of the modelled beams and the lowest elastic buckling mode with an odd number of buckling half-waves [11,12,26] under the considered loading conditions was employed to simulate the distribution of local imperfections. A sensitivity study was performed to investigate the influence of various incorporated imperfection amplitudes ω_0 on the response of the hot-rolled and cold-formed steel continuous beams and seek the most appropriate value to be used in the subsequent parametric studies. Four local imperfection amplitudes, defined as the fractions of the flat width of flange b (b/100, b/200, b/300 and b/400), were considered in the FE models.

The boundary conditions of the FE models were carefully defined to simulate the test setup described in [4]. The centre points of the bottom faces of the cross-sections in the support and loading regions were coupled to all the nodes within the corresponding cross-section, where wooden blocks were placed to prevent web crippling, with boundary conditions applied at each centre point to allow appropriate movement and rotation. At the central support of the continuous beams, all degrees of freedom were restrained apart from rotation about the axis of bending, while at the end support, similar boundary conditions to those applied at the central support were adopted, but allowing for the longitudinal movement. The concentrated loads on each span of the continuous beams were simulated as imposed vertical displacements. Following the elastic buckling analysis and incorporation of the representative initial local geometric imperfections into the FE models, nonlinear static analyses were performed to obtain

the ultimate loads and rotation capacities of the continuous beams, using the modified Risks method [20].

3.2. Validation of the FE models

The accuracy of the FE models was evaluated by comparing their ultimate loads, full load-end rotation histories and failure modes against those observed in the experiments [4]. The ultimate loads obtained from the FE models $F_{u,FE}$, considering the different conditions for corner strength enhancement (for the cold-formed sections) and imperfection amplitudes, have been normalized by the corresponding experimental ultimate loads $F_{u,test}$, and reported in Tables 3 and 4 for the hot-rolled and cold-formed steel continuous beams, respectively, together with the mean values and the coefficients of variation (COV) of the $F_{u,FE}/F_{u,test}$ ratios. It may be observed that the ultimate loads $F_{u,FE}$ derived from the FE models were insensitive to variation in the imperfection amplitudes for both the hot-rolled and cold-formed steel continuous beams, while the extent of corner strength enhancement was shown to be more influential on the numerically obtained results, as indicated in Table 4. The FE results showed good accuracy and consistency in predicting the experimental results when the local imperfection amplitude of $b/200$ for both the hot-rolled and cold-formed steel sections and the enhanced strength region extended to a distance of $2t$ for the cold-formed steel sections were employed. Adoption of these parameters in the FE models led to the mean ratios of $F_{u,FE}/F_{u,test}$ equal to 1.03 and 0.98, with the corresponding COVs of 0.050 and 0.025, for the hot-rolled and cold-formed steel continuous beams, respectively. Typical examples of load-end rotation (F-θ) curves are compared in Figs 4 and 5 for hot-rolled and cold-formed steel continuous beams, respectively, showing that the general shape of the full experimental load-deformation histories is accurately replicated by the FE simulations. The failure modes observed in the test specimens were also well predicted by the FE models; both failure modes consist of three distinct plastic hinges at

the central support and loading points, formed with different sequences due to different loading configurations, and displaying inelastic local buckling for some beams at large deformations. A typical comparison of failure modes obtained from a tested and simulated continuous beam specimen is shown in Fig. 6. Overall, the FE models were found to be capable of simulating the structural performance of both hot-rolled and cold-formed steel continuous beams, and were thus considered suitable for conducting parametric studies.

3.3. Parametric studies

Following validation of the FE models, an extensive parametric study was performed to provide further data on hot-rolled and cold-formed steel SHS and RHS continuous beams over a wider range of cross-section geometries, cross-section slendernesses, steel grades and loading conditions for the purpose of assessing and developing plastic design methods. A range of SHS and RHS, with the cross-section aspect ratios of the latter ranging from 1.3 to 2.0, was considered in the parametric study. The outer width (B) of the modelled SHS was varied between 50 mm and 140 mm, whereas for the RHS, the outer width (B) was varied from 60 mm to 80 mm while the outer height (H) was varied between 80 mm and 160 mm. The internal corner radii (r_i) of the cross-sections were set equal to the wall thickness (t), which was varied between 1.5 mm and 11 mm, resulting in a wide spectrum of cross-section slenderness values $\overline{\lambda}_p$ (i.e. determined using CUFSM [27]), but within the range of non-slender cross-sections ($\overline{\lambda}_p \leq 0.68$), which are the focus of the present study. The overall beam length of 3200 mm, with each span length equal to 1500 mm (and 100 mm overhang at each end), was kept constant, while the position of the applied load was varied to generate three loading configurations (L_2 = 500 mm, 750 mm and 1000 mm, designated as "1/3 Span", "1/2 Span" and "2/3 Span", respectively).

Two different steel grades, namely S355 and S460, with the nominal yield strength of 355 N/mm^2 and 460 N/mm^2, respectively, were adopted in the parametric studies for both the hot-rolled and cold-formed members. A bilinear plus nonlinear hardening material model for hot-rolled steels [2] and a two-stage Ramberg-Osgood material model for cold-formed steels [3] were adopted to represent the full stress-strain curves used in the parametric study; the employed material parameters for the considered hot-rolled and cold-formed steel grades are summarised in Tables 5 and 6, respectively, including the Young's modulus E, the yield strength (taken as the 0.2% proof stress for the cold-formed steels) f_y, the ultimate tensile strength f_u, the ultimate strain ε_u and the strain hardening exponents n and m. Since the enhanced yield strength of the corner material depends on the geometric properties of the corners [3,28], which varied among the considered sections, an average enhancement in corner yield strength of 25% over the corresponding flat yield strength [3] was adopted for all cross-sections in the parametric studies for modelling convenience. The adopted stress-strain curves for the hot-rolled and cold-formed steel sections are illustrated in Figs 7 and 8, respectively. A total of 2690 models were analysed, with 1345 for each production route, which included two steel grades and three loading configurations, to obtain a thorough understanding of the inelastic behaviour and moment redistribution in hot-rolled and cold-formed SHS and RHS continuous beams.

4. Discussion and assessment of design methods for indeterminate structures

In this section, the ultimate loads $F_{u,FE}$ generated from the parametric study together with the experimental ultimate loads $F_{u,test}$ obtained from [4] are utilized to assess the accuracy of the current design provisions of EN 1993-1-1 [1] and the continuous strength method (CSM) [11,12,17-19] in predicting the capacity of hot-rolled and cold-formed steel SHS and RHS indeterminate structures. Note that the comparisons performed in the present study are based

on the measured (or modelled) geometries and material properties (using area-weighted average material properties for the cold-formed sections), and all partial safety factors are set equal to unity.

4.1. European design specification: EN 1993-1-1 (EC3)

The design approach for hot-rolled and cold-formed steel SHS and RHS set out in EN 1993-1-1 [1] follows the traditional concept of cross-section classification, which is based on the assumption of elastic, perfectly-plastic material model, with no distinction made between sections from different production routes at the level of cross-section design. In EN 1993-1-1, the bending resistance of a cross-section ($M_{u,EC3}$) is determined on the basis of its classification – for Class 1 and 2 sections, the plastic moment capacity M_{pl} is employed; for Class 3 sections, the elastic moment capacity M_{el} is used; finally for Class 4 sections, effective section properties need to be considered and a lower effective moment capacity M_{eff} is determined.

With regards to the design of indeterminate structures, global plastic analysis, in which a sequence of plastic hinges forms under increasing loading until a collapse mechanism is achieved, can be employed for structures with Class 1 cross-sections. For the continuous beams analysed in the present study, the ultimate load F_u determined based on global plastic analysis is equivalent to the theoretical load causing a collapse mechanism with the plastic moment capacity M_{pl} reached at each hinge. The global plastic analysis allows redistribution of bending moments, thus enabling the exploitation of the reserve strength in continuous beams due to their statical indeterminacy. However, the global plastic design is limited to Class 1 sections, which are assumed to be able to maintain their plastic moment capacity while undergoing sufficient rotations to allow full redistribution of moments. For continuous beams with Class 2, 3 or 4 sections, the ultimate resistance is calculated based on global elastic analysis, which

assumes that structural collapse occurs when the most critical cross-section (i.e. the most heavily loaded cross-section) reaches its corresponding cross-section bending resistance, with moment redistribution not being considered.

The ultimate loads obtained from both the experiments $F_{u,test}$ [4] and FE simulations $F_{u,FE}$ were used to assess the accuracy of the codified design provisions of EC3 [1], as shown in Figs 9 and 10 for hot-rolled and cold-formed steel continuous beams, respectively. In these figures, the experimental and numerical ultimate loads have been normalised with respect to the predicted ultimate load determined from EC3 ($F_{u,EC3}$) and plotted against the cross-section slenderness $\overline{\lambda}_p$, determined on an element-by-element basis and taken, according to EC3, as the slenderness of the most slender plate element in the cross-section. The Class 1 to 3 slenderness limits for internal elements in compression specified in EC3 are also shown in Figs 9 and 10, to indicate the points at which the design model changes. The EC3 ultimate load predictions for the hot-rolled and cold-formed steel SHS and RHS continuous beams with Class 1 sections may be seen to be generally conservative, and the conservatism increases with decreasing cross-section slenderness, due largely to the neglect of the beneficial effects of strain hardening at the cross-sectional level. For the grade S355 steel, which exhibits a higher degree of strain hardening compared with the grade S460 steel, a more pronounced level of conservatism is observed in the EC3 predictions for the more stocky sections (i.e. sections with lower $\overline{\lambda}_p$), as shown in Figs 9 and 10; however, for the less stocky sections where strain hardening is less or even not experienced, the differences between the two steel grades diminish. A quantitative evaluation of the EC3 design approach can be found in Tables 7 and 8, which show the mean FE (test)-to-EC3 predicted ultimate load ratios $F_{u,FE(test)}/F_{u,EC3}$ of 1.18 and 1.22, with corresponding COVs of 0.11 and 0.06, for hot-rolled and cold-formed steel Class 1 SHS and RHS continuous beams, respectively. The EC3 predictions for the Class 2 and 3 cross-

sections, for which elastic global analysis is used, are generally seen to be overly conservative, due largely to the lack of account taken of bending moment redistribution. Moreover, a discontinuity arises at the border between Class 2 and Class 3 sections, giving rise to conservatism in the estimation of the ultimate loads of Class 3 sections, since the bending resistances of Class 3 sections are limited to their elastic bending moments M_{el}, without considering the partial spread of plasticity. A similar trend was observed for all the analysed test configurations, though the EC3 predictions for the continuous beams loaded in the "1/3 Span" configuration, which benefit to the greatest extent from moment redistribution (i.e. they have the highest ratio of plastic collapse load to first hinge load), were found to be the most conservative, followed by the "1/2 Span" and then the "2/3 Span" configurations. As reported in Tables 7 and 8, the mean ratios of FE (test) to EC3 predicted strength for Class 2 and 3 SHS and RHS continuous beams are equal to 1.27 for hot-rolled steel and 1.34 for cold-formed steel, with corresponding COVs of 0.14 and 0.15, respectively.

4.2. Continuous strength method (CSM)

From the above comparisons, it may be observed that the current design rules in EN 1993-1-1 provide overly conservative ultimate load predictions for both hot-rolled and cold-formed steel continuous beams; this is attributed to the lack of account for strain hardening, which results in under-predictions of bending resistance at the cross-sectional level, especially for the more stocky sections [11,12], and the neglect of bending moment redistribution at the system level beyond Class 1 sections. The bending resistance of Class 3 sections is also under-predicted when based on the elastic moment capacity M_{el} [11,12]. To address this shortcoming, the continuous strength method (CSM) has been developed and thoroughly validated as an alternative design approach that rationally exploits material strain hardening and the spread of plasticity at the cross-sectional level [11,12], and this method has recently been extended to

indeterminate stainless steel [16-18] and aluminium alloy structures [19], which combines the merits of traditional plastic analysis (i.e. allowing for moment redistribution) and the CSM for determining the cross-section bending resistance (i.e. allowing for strain hardening and the spread of plasticity). In this section, the CSM for the design of hot-rolled and cold-formed steel cross-sections is summarized [11,12] and its application to hot-rolled and cold-formed steel continuous beams is further explained and assessed.

4.2.1. CSM for cross-section design

The continuous strength method (CSM) is a deformation based design approach that employs a 'base curve' to determine the maximum strain ε_{csm} that a cross-section can reach, in conjunction with a material model that allows for the beneficial influence of strain hardening, to determine the cross-section resistances. The base curve is defined by Eq. (3) for non-slender cross-sections (i.e. $\bar{\lambda}_p \le 0.68$), where ε_y is the material yield strain equal to f_y/E and $\bar{\lambda}_p$ is the cross-section slenderness, which is defined in a non-dimensional form by Eq. (4). In Eq. (4), σ_{cr} is the elastic buckling stress under the applied loading conditions and should preferably be determined for the full cross-section, using analytical or numerical methods, which account for element interaction effects. The finite strip software CUFSM [27] was employed herein. Note that the base curve, as given by Eq. (3), applies to cross-sections with $\bar{\lambda}_p$ less than or equal to 0.68, which is defined as the boundary between non-slender and slender cross-sections [29].

$$\frac{\varepsilon_{csm}}{\varepsilon_y} = \frac{0.25}{\bar{\lambda}_p^{3.6}} \quad \text{but} \quad \frac{\varepsilon_{csm}}{\varepsilon_y} \le \min\left(15, \frac{C_1\varepsilon_u}{\varepsilon_y}\right), \quad \text{for } \bar{\lambda}_p \le 0.68 \tag{3}$$

$$\bar{\lambda}_p = \sqrt{f_y / \sigma_{cr}} \tag{4}$$

The differences in material properties between hot-rolled and cold-formed steels are recognised in the CSM by adopting different stress-strain relationships, reflecting their particular strain hardening characteristics. The first three stages of the quad-linear material model proposed in [2], as illustrated in Fig. 11 and described by Eq. (5), is adopted as the CSM material model for hot-rolled carbon steels [11], taking account of both the yield plateau and the strain hardening.

$$f(\varepsilon) = \begin{cases} E\varepsilon & \text{for } \varepsilon \le \varepsilon_{\mathrm{y}} \\ f_{\mathrm{y}} & \text{for } \varepsilon_{\mathrm{y}} < \varepsilon \le \varepsilon_{\mathrm{sh}} \\ f_{\mathrm{y}} + E_{\mathrm{sh}}(\varepsilon - \varepsilon_{\mathrm{sh}}) & \text{for } \varepsilon_{\mathrm{sh}} < \varepsilon \le C_1\varepsilon_{\mathrm{u}} \\ f_{C_1\varepsilon_{\mathrm{u}}} + \dfrac{f_{\mathrm{u}} - f_{C_1\varepsilon_{\mathrm{u}}}}{\varepsilon_{\mathrm{u}} - C_1\varepsilon_{\mathrm{u}}}(\varepsilon - C_1\varepsilon_{\mathrm{u}}) & \text{for } C_1\varepsilon_{\mathrm{u}} < \varepsilon \le \varepsilon_{\mathrm{u}} \text{ (not used in the CSM)} \end{cases} \quad (5)$$

Four material coefficients (C_1, C_2, C_3 and C_4) are used in the material model: C_1 defines a 'cut-off' strain to avoid over-predictions of material strength and is also included in the CSM base curve (Eq. (3)); C_2 is employed in Eq. (6) to determine the strain hardening slope E_{sh}; and C_3 and C_4 are used in the predictive expression for ultimate strain ε_{u} (see Eq. (7)), which is also needed for the determination of E_{sh}. The strain hardening strain $\varepsilon_{\mathrm{sh}}$ for hot-rolled steels may be determined from Eq. (8), which has been calibrated based on a large set of experimental database by Yun and Gardner [2]. Note that the quad-linear material model adopts the same definitions for the material coefficients as used in the elastic, linear hardening CSM material model, which has been employed throughout the development of the CSM to represent the strain hardening response of materials with rounded stress-strain behaviour, such as stainless steels, aluminium and cold-formed steels, and can indeed be seen as a superset of the previous model. Unlike the quad-linear material model, the CSM elastic, linear hardening material model has no yield plateau (see Fig. 12), resulting in E_{sh} being defined by Eq. (9). Recommended values or predictive expressions for the coefficients C_{i} for different materials

are summarized in Table 9. Detailed information on the derivation of these coefficients is given in [2,10,12,15,29,30].

$$E_{sh} = \frac{f_u - f_y}{C_2\varepsilon_u - \varepsilon_{sh}} \quad \text{for hot-rolled carbon steels} \tag{6}$$

$$\varepsilon_u = C_3\left(1 - \frac{f_y}{f_u}\right) + C_4 \quad \text{but } \varepsilon_u \geq 0.06 \text{ for hot-rolled carbon steels} \tag{7}$$

$$\varepsilon_{sh} = 0.1\frac{f_y}{f_u} - 0.055 \quad \text{but } 0.015 \leq \varepsilon_{sh} \leq 0.03 \tag{8}$$

$$E_{sh} = \frac{f_u - f_y}{C_2\varepsilon_u - \varepsilon_y} \quad \text{for materials with rounded stress-strain behaviour} \tag{9}$$

$$C_1 = \frac{\varepsilon_{sh} + 0.25(\varepsilon_u - \varepsilon_{sh})}{\varepsilon_u} \quad \text{for hot-rolled carbon steels} \tag{10}$$

$$C_2 = \frac{\varepsilon_{sh} + 0.4(\varepsilon_u - \varepsilon_{sh})}{\varepsilon_u} \quad \text{for hot-rolled carbon steels} \tag{11}$$

The design formulae for the CSM cross-section bending resistance $M_{csm,Rd}$ can be derived based on the assumptions of a linearly-varying strain distribution throughout the depth of the cross-section and the corresponding CSM material models. For cold-formed steel SHS/RHS, $M_{csm,Rd}$ can be obtained from Eq. (12) [31], where W_{el} is the elastic section modulus, W_{pl} is the plastic section modulus and γ_{M0} is a partial safety factor for cross-section resistance, with a recommended valued of unity for structural steels.

$$M_{\mathrm{csm,Rd}} = \frac{W_{\mathrm{pl}} f_{\mathrm{y}}}{\gamma_{\mathrm{M0}}} \left[1 + \frac{E_{\mathrm{sh}}}{E} \frac{W_{\mathrm{el}}}{W_{\mathrm{pl}}} \left(\frac{\varepsilon_{\mathrm{csm}}}{\varepsilon_{\mathrm{y}}} - 1 \right) - \left(1 - \frac{W_{\mathrm{el}}}{W_{\mathrm{pl}}} \right) \left(\frac{\varepsilon_{\mathrm{csm}}}{\varepsilon_{\mathrm{y}}} \right)^{-2} \right] \tag{12}$$

For hot-rolled steel sections, two scenarios need to be considered in determining the CSM cross-section resistance in bending $M_{\mathrm{csm,Rd}}$. For the less stocky cross-sections, where strain hardening is not experienced (i.e. $\varepsilon_{\mathrm{csm}} \leq \varepsilon_{\mathrm{sh}}$), the design formula for hot-rolled steel SHS/RHS in bending is the same as that derived for cold-formed steel SHS/RHS using the bi-linear CSM material model (see Eq. (12)), with E_{sh} taken equal to zero to represent the yield plateau; this leads to a simpler expression, as given by Eq. (13).

$$M_{\mathrm{csm,Rd}} = \frac{W_{\mathrm{pl}} f_{\mathrm{y}}}{\gamma_{\mathrm{M0}}} \left[1 - \left(1 - \frac{W_{\mathrm{el}}}{W_{\mathrm{pl}}} \right) \left(\frac{\varepsilon_{\mathrm{csm}}}{\varepsilon_{\mathrm{y}}} \right)^{-2} \right] \tag{13}$$

For the more stocky sections, where $\varepsilon_{\mathrm{csm}} > \varepsilon_{\mathrm{sh}}$, the outer fibre of the cross-section will enter into the strain hardening regime and some benefit from strain hardening can be exploited. In this case, the CSM bending resistance for hot-rolled steel SHS/RHS can be predicted from Eq. (14) [11]. Note that Eq. (14) was developed based on the first three stages of the quad-linear material model (see Eq. (5) and Fig. 11); the strain hardening slope E_{sh} employed in Eq. (14) should therefore be determined using Eq. (6). A detailed account of the latest developments to the CSM for hot-rolled and cold-formed steel cross-sections under different loading conditions can be found in [11,12,32,33].

$$M_{\mathrm{csm,Rd}} = \frac{W_{\mathrm{pl}} f_{\mathrm{y}}}{\gamma_{\mathrm{M0}}} \left[1 - \left(1 - \frac{W_{\mathrm{el}}}{W_{\mathrm{pl}}} \right) \left(\frac{\varepsilon_{\mathrm{csm}}}{\varepsilon_{\mathrm{y}}} \right)^{-2} + 0.1 \left(\frac{\varepsilon_{\mathrm{csm}} - \varepsilon_{\mathrm{sh}}}{\varepsilon_{\mathrm{y}}} \right)^{2} \frac{E_{\mathrm{sh}}}{E} \right] \tag{14}$$

The CSM for the design of hot-rolled and cold-formed steel sections has been shown to provide more accurate and consistent predictions of cross-section bending resistances [11,12] than EC3, and thus improved design rules for the continuous beams may be sought through the use of the CSM bending moment capacity predictions and a rational allowance for moment redistribution in a similar fashion to traditional plastic analysis, as outlined and discussed in the following sub-section.

4.2.2. CSM for indeterminate structures

Extension of the CSM to the design of indeterminate structures has recently been proposed, and assessed using experimental and numerical data on stainless steel and aluminium continuous beams [16-19]. The method was shown to provide more accurate and consistent predictions of the ultimate load of continuous beams than conventional plastic design, especially for more stocky cross-sections, by accounting for both strain hardening and moment redistribution in the strength calculation. Structural carbon steels exhibit different stress-strain characteristics compared to stainless steels and aluminium alloys and, as a result, extension of the scope of the method to the design of hot-rolled and cold-formed steel continuous beams requires careful assessment.

The CSM for indeterminate structures considers moment redistribution by means of assigning the CSM cross-section bending resistance M_{csm} to the critical hinge (i.e. the hinge showing the largest rotation capacity demand) and reduced CSM cross-section bending resistances to the subsequent hinges, recognising the lower level of rotation demands in the considered collapse mechanism. This approach provides a more rational basis for allowing for moment redistribution than traditional plastic analysis, which simply assigns the plastic moment capacity M_{pl} to all hinges, without accounting for the varying rotation demands at the different

hinges. Following analysis of the experimental and numerical data, the CSM design approach for determining the resistance of hot-rolled and cold-formed steel indeterminate structures is proposed herein. The rotation demand α_i of each hinge in the considered collapse mechanism is calculated using Eq. (15), where θ_i is the hinge rotation based on kinematic considerations related to the collapse mechanism, H_i is the section height at the considered location and $(\varepsilon_{csm}/\varepsilon_y)_i$ is the corresponding normalised strain ratio at hinge i. In the case of five-point bending with symmetrical point loads and constant cross-section geometry, which is the focus of the present paper, the cross-section height H_i and the strain ratios $(\varepsilon_{csm}/\varepsilon_y)_i$ remain constant along the member length. The hinge rotations at the loading positions θ_1 and at the central support position θ_2, derived based on the considered collapse mechanism illustrated in Fig. 13, are equal to $(\delta/L_1+ \delta/L_2)$ and $2\delta/L_2$, respectively. For those loading configurations where the distance between the point load and the central support is less than half of the span (i.e. $L_2 < L_s/2$), the critical hinge is at the central support, while in the loading configurations where $L_2 > L_s/2$, the critical hinges form simultaneously at the two loading points; for $L_2 = L_s/2$, all hinges (i.e. at the central support and two loading points) form simultaneously. The critical hinge has the highest hinge rotation demand α_{max} and its deformation capacity (i.e. $\varepsilon_{csm}/\varepsilon_y$) is assumed to be fully achieved. For the remaining hinges, reduced deformation capacities $(\varepsilon_{csm}/\varepsilon_y)_{i,R}$ are assigned in proportion to the rotation demand ratios, but with upper bound limits, as given in Eq. (16). These limits prevent excessive deformations and over-predictions of material strength, and are consistent with the CSM base curve (see Eq. (3)).

$$\alpha_i = \frac{\theta_i h_i}{(\varepsilon_{csm} / \varepsilon_y)_i} \tag{15}$$

$$\left(\frac{\varepsilon_{csm}}{\varepsilon_y}\right)_{i,R} = \frac{\alpha_i}{\alpha_{max}}\left(\frac{\varepsilon_{csm}}{\varepsilon_y}\right)_i \quad \text{but} \quad \left(\frac{\varepsilon_{csm}}{\varepsilon_y}\right)_{i,R} \le \min\left(15, \frac{C_1\varepsilon_u}{\varepsilon_y}\right) \tag{16}$$

Once the deformation capacity of each hinge is identified (i.e. $(\varepsilon_{csm}/\varepsilon_y)_{i,R}$), the corresponding CSM bending resistance can be calculated from Eq. (12) for cold-formed steel sections and from Eq. (13) or Eq. (14) for hot-rolled steel sections when $(\varepsilon_{csm}/\varepsilon_y)_{i,R}$ is greater than or equal to unity. For $(\varepsilon_{csm}/\varepsilon_y)_{i,R} < 1$, the reduced CSM bending resistance $M_{csm,Rd}$ at hinge i can be calculated by the product of the reduced CSM strain ratio $(\varepsilon_{csm}/\varepsilon_y)_{i,R}$ and the elastic section modulus W_{el}, as given by Eq. (17).

$$M_{csm,Rd} = \left(\frac{\varepsilon_{csm}}{\varepsilon_y}\right)_{i,R} \frac{W_{el}}{\gamma_{M0}} \tag{17}$$

Finally, the ultimate collapse load of the considered system is determined by means of virtual work, by equating the external work done by the applied loads F_j acting through virtual displacements δ_j to the internal work resulting from the hinge rotations θ_i (see Eq. (18)). Note that for more complex structural systems with higher degrees of statical indeterminacy, all possible collapse mechanisms should be considered in order for the critical mechanism to be identified.

$$\sum_j F_j \delta_j = \sum_i M_i \theta_i \tag{18}$$

Previous studies [16-19,31] suggest that the CSM for indeterminate structures is applicable to box-sections with $\bar{\lambda}_p \le 0.48$, which corresponds to a normalised deformation capacity $(\varepsilon_{csm}/\varepsilon_y)$ of 3.6, according to the CSM base curve (see Eq. (3)), while global elastic analysis should be used for box-sections with $\bar{\lambda}_p > 0.48$. Following analysis of the numerical results generated herein, the slenderness limit of 0.48 is considered to be rather conservative, as illustrated in Figs 14 and 15, where the FE (or test) to CSM predicted ultimate load (using the plastic design

method described in this section) ratio $F_{u,FE(test)}/F_{u,csm}$ is plotted against the cross-section slenderness $\bar{\lambda}_p$ for the hot-rolled steel and cold-formed steel continuous beams, respectively. It is recommended herein that this limit be relaxed to 0.60 for both hot-rolled and cold-formed steel continuous beams. This proposed slenderness limit for plastic design is more relaxed in the CSM than in EC3, since traditional plastic design in EC3 assumes that plastic hinges achieve their plastic bending moment M_{pl} and have a rotation capacity of at least R = 3. However, in the CSM, firstly the hinges have a reduced moment capacity with increasing slenderness and secondly, direct allowance is made for the actual rotation demands at each hinge by considering the kinematics of the analysed collapse mechanism, both of which justify the allowance for some degree of moment redistribution for more slender cross-sections.

The CSM plastic design proposals are evaluated by comparing the experimental and numerical ultimate loads against their corresponding CSM ultimate load predictions. As shown in Tables 7 and 8, the mean ratios of $F_{u,FE(test)}/F_{u,csm}$ for cross-sections with $\bar{\lambda}_p \leq 0.60$, above which CSM plastic design would not be applicable, are equal to 1.17 for both hot-rolled and cold-formed steel continuous beams, with COVs of 0.09 and 0.03, respectively; relative to EC3, the CSM provides both more accurate and more consistent (i.e. lower COV values) resistance predictions. However, as is evident in Fig. 14 and Table 7, the CSM predictions remain conservative for hot-rolled steel continuous beams with the stocky cross-sections (e.g. $\bar{\lambda}_p \leq 0.32$); this is due primary to the imposed upper bound limit to the strain ratio of $\varepsilon_{csm}/\varepsilon_y$ = 15. This limit prevents the full exploitation of strain hardening in hot-rolled steel sections since, due to the presence of the yield plateau, rather high levels of strain must be attained before the initiation of strain hardening. This limit could, however, be adjusted depending on the level of plastic deformation that was deemed acceptable at the ultimate limit state in a given project. Table 7 also gives the mean and COV values of $N_{u,FE(test)}/N_{u,csm}$ when the CSM strain ratio is relaxed to 25, revealing

improved accuracy and reduced scatter over the CSM with the stricter strain ratio limit of 15; this improvement is also illustrated in Fig. 16, where the $F_{u,FE(test)}/F_{u,csm}$ ratio based on $\varepsilon_{csm}/\varepsilon_y \leq 25$ is plotted against $\overline{\lambda}_p$. The CSM plastic design proposals allow for the rational exploitation of strain hardening, with average enhancements in ultimate load predictions of 4% and 6% for hot-rolled and cold-formed steel SHS and RHS continuous beams with Class 1 sections compared with the traditional plastic design in EC3, as shown in Tables 7 and 8.

5. Reliability analysis

Statistical analyses in accordance with the provisions of EN 1990 [34] were performed to evaluate the reliability of the current EC3 provisions and the proposed CSM for the plastic design of hot-rolled and cold-formed steel SHS and RHS continuous beams, on the basis of the experimental and numerical results. The key calculated statistical parameters for both design approaches are summarized in Table 10, where $k_{d,n}$ is design (ultimate limit state) fractile factor that is related to the number of test or numerical results in the comparison database, b is the mean ratio of test and numerical resistances to predicted resistances, V_δ is the COV of the test and numerical resistances relative to the resistance model, V_r is the combined COV incorporating both model and basic variable uncertainties and γ_{M0} is the partial safety factor with a recommended value of unity for the design of hot-rolled and cold-formed steel SHS and RHS in EN 1993-1-1 [1]. A calculated partial safety less than unity therefore indicates that the reliability requirements of EN 1990 [34] are met when a value of $\gamma_{M0} = 1.0$ is employed with the resistance function. In the present reliability analysis, the mean-to-nominal ratios of yield strength and geometric properties were taken as 1.16 and 1.00, with corresponding COVs of 0.05 and 0.03, for both hot-rolled and cold-formed steels, following the recommendations of Byfield and Nethercot [35]. Similar values were adopted in a recent study by Tankova et al. [36].

According to the results reported in Table 10, the partial safety factor γ_{M0} for the proposed CSM with strain ratio limit of 15 is slightly larger than unity for the hot-rolled steel continuous beams and is less than unity for the cold-formed steel continuous beams, but all values are very close to unity and lower than those obtained from EC3, demonstrating that the CSM plastic design proposal can be used safely. The CSM partial safety factor for hot-rolled steel continuous beams can, however, be further reduced by relaxing the strain ratio limit to 25, whereby the scatter of the design predictions is significantly reduced (i.e. lower V_δ value). The existing EC3 plastic design approach meets the Eurocode reliability requirements for cold-formed steel continuous beams, but its partial safety factor is larger than the target value of 1.0 for hot-rolled steel SHS and RHS continuous beams.

6. Conclusions

A comprehensive numerical investigation into the structural performance of hot-rolled and cold-formed steel continuous beams with square and rectangular hollow sections has been presented. Finite element (FE) models were first developed and validated against existing test results. Following validation of the FE models, parametric studies were performed, generating a total of 2690 numerical results on hot-rolled and cold-formed steel continuous beams, covering a wide range of cross-section geometries, cross-section slendernesses, steel grades and loading conditions. Both the numerical results generated in the present paper and the test data obtained from [4] were then used to assess the accuracy of the provisions of EN 1993-1-1 and CSM proposals for the design of hot-rolled and cold-formed steel SHS and RHS continuous beams. The current EN 1993-1-1 provisions were found to be rather conservative in predicting the ultimate capacity of both hot-rolled and cold-formed steel continuous beams, especially for very stocky sections and Class 3 sections. The conservatism in EN 1993-1-1 can be attributed to the neglect of strain hardening for the stocky sections and the partial spread of

plasticity for Class 3 sections at the cross-sectional level, and the lack of account for moment redistribution for Class 2 and 3 sections at the global system level. The CSM proposal considers strain hardening and allows for moment redistribution in a continuous way, resulting in improved accuracy and reduced scatter over the EN 1993-1-1 design provisions. Finally, reliability analyses were conducted according to the EN 1990 requirements [34], and it was found that the proposed CSM can be safely applied to the plastic design of hot-rolled and cold-formed steel SHS and RHS continuous beams with cross-section slenderness $\overline{\lambda}_{\mathrm{p}} \leq 0.60$; moreover, the CSM strain ratio limit can be safely relaxed to 25 to achieve more accurate ultimate load predictions for hot-rolled steel continuous beams, though it is recommended that an upper limit on the acceptable level of normalised strain ($\varepsilon_{\mathrm{csm}}/\varepsilon_{\mathrm{y}}$) be defined on a project by project basis. Consideration of a wider range of indeterminate structural configurations under various loading conditions is required in future work.

Acknowledgements

The first author is supported by a scholarship from the China Scholar Council (CSC); this support is gratefully appreciated.

References

[1] EN 1993-1-1. Eurocode 3: Design of steel structures − Part 1–1: General rules and rules for buildings. Brussels: European Committee for Standardization (CEN); 2005.

[2] Yun X, Gardner L. Stress-strain curves for hot-rolled steels. Journal of Constructional Steel Research 2017;133:36-46.

[3] Gardner L, Yun X. Description of stress-strain curves for cold-formed steel. Construction and Building Materials (Under review).

[4] Gardner L, Saari N, Wang F. Comparative experimental study of hot-rolled and cold-formed rectangular hollow sections. Thin-Walled Structures 2010;48(7):495-507.

[5] Zhao XL, Wilkinson TJ, Hancock GJ. Cold-formed tubular members and connections – Structural behaviour and design. Elsevier, London, 2005.

[6] Ma JL, Chan TM, Young B. Material properties and residual stresses of cold-formed high strength steel hollow sections. Journal of Constructional Steel Research 2015;109:152-165.

[7] Zhang XZ, Liu S, Zhao MS, Chiew SP. Comparative experimental study of hot-formed, hot-finished and cold-formed rectangular hollow sections. Case Studies in Structural Engineering 2016;6:115-129.

[8] Nseir J. Development of a new design method for the cross-section capacity of steel hollow sections. PhD thesis, Université de Liège, Liège, Belgium; 2015.

[9] AISC 360-16. Specification for structural steel buildings. Chicago, IL: American Institute of Steel Construction (AISC); 2016.

[10] Gardner L, Yun X, Macorini L, Kucukler M. Hot-rolled steel and steel-concrete composite design incorporating strain hardening. Structures 2017;9:21-28.

[11] Yun X, Gardner L, Boissonnade N. The continuous strength method for the design of hot-rolled steel cross-sections. Engineering Structures 2018;157:179-191.

[12] Yun X, Gardner L. The continuous strength method for the design of cold-formed steel cross-sections. Engineering Structures (under review).

[13] Byfield MP, Nethercot DA. An analysis of the true bending strength of steel beams. Proceedings of Institution of Civil Engineers. Structures and Buildings 1998;128(2):188-197.

[14] Wilkinson T, Hancock GJ. Tests to examine compact web slenderness of cold-formed RHS. Journal of Structural Engineering ASCE 1998;124(10):1166-1174.

[15] Afshan S, Gardner L. The continuous strength method for structural stainless steel design. Thin-Walled Structures 2013;68:42-49.

[16] Theofanous M, Saliba N, Zhao O, Gardner L. Ultimate response of stainless steel continuous beams. Thin-Walled Structures 2014;83:115-127.

[17] Arrayago I, Real E, Mirambell E. Design of stainless steel continuous beams with tubular cross-sections. Engineering Structures 2017;151:422-431.

[18] Gkantou M, Kokosis G, Theofanous M, Dirar S. Plastic design of stainless steel continuous beams. Journal of Constructional Steel Research 2018; (in press).

[19] Su MN, Young B, Gardner L. Continuous beams of aluminum alloy tubular cross sections. II: parametric study and design. Journal of Structural Engineering ASCE 2014;141(9):04014233.

[20] ABAQUS. Analysis user's manual, Version 6.14. Dassault systems; 2014.

[21] Karren KW. Corner properties of cold-formed shapes. Journal of the Structural Division ASCE 1967;93(1):401-433.

[22] Ma JL, Chan TM, Young B. Material properties and residual stresses of cold-formed high strength steel hollow sections. Journal of Constructional Steel Research 2015;109:152-165.

[23] ECCS. Ultimate limit state calculation of sway framed with rigid joints. Technical Committee 8 of European Convention for Constructional Steelwork (ECCS), First Edition, No. 33;1984.

[24] Tall L. Recent developments in the study of column behaviour. Journal of The Institution of Engineers 1964;36(12):319-333.

[25] Ashraf M, Gardner L, Nethercot DA. Finite element modelling of structural stainless steel cross-sections. Thin-walled structures 2006;44(10):1048-1062.

[26] Silvestre N, Gardner L. Elastic local post-buckling of elliptical tubes. Journal of Constructional Steel Research 2011;67:281-292.

[27] Schafer BW, Ádány S. Buckling analysis of cold-formed steel members using CUFSM: conventional and constrained finite strip methods. Proceedings of the 18th International

Specialty Conference on Cold-formed Steel Structures 26-27 October 2006, Orlando, Florida, USA, 39-54.

[28] Rossi B, Afshan S, Gardner L. Strength enhancements in cold-formed structural sections − Part II: Predictive models. Journal of Constructional Steel Research 2013;83:189-196.

[29] Bock M, Gardner L, Real E. Material and local buckling response of ferritic stainless steel sections. Thin-Walled Structures 2015;89:131-141.

[30] Su MN, Young B, Gardner L. The continuous strength method for the design of aluminium alloy structural elements. Engineering Structures 2016;122:338-348.

[31] Gardner L, Wang F, Liew A. Influence of strain hardening on the behaviour and design of steel structures. International Journal of Structural Stability and Dynamics 2011;11(05):855-875.

[32] Yun X, Gardner L, Boissonnade N. Ultimate capacity of I-sections under combined loading – Part 1: Experiments and FE model validation. Journal of Constructional Steel Research 2018;147:408-421.

[33] Yun X, Gardner L, Boissonnade N. Ultimate capacity of I-sections under combined loading – Part 2: Parametric studies and CSM design. Journal of Constructional Steel Research 2018; (in press).

[34] EN 1990. Basis of structural design. Brussels: European Committee for Standardization (CEN); 2002.

[35] Byfield MP, Nethercot DA. Material and geometric properties of structural steel for use in design. The Structural Engineer 1997;75:363-367.

[36] Tankova T, da Silva LS, Marques L, Rebelo C, Taras A. Towards a standardized procedure for the safety assessment of stability design rules. Journal of Constructional Steel Research 2014;103:290-302.

Tables:

Table 1: Measured dimensions of continuous beam specimens [4].

Continuous beam specimen	Test configuration	B	H	t	r_i	W_{el}	W_{pl}
		mm	mm	mm	mm	mm^3	mm^3
RHS 60×40×4 HR1	1/2 Span	40.27	60.09	3.85	1.91	10500	13300
RHS 60×40×4 HR2	1/3 Span	40.33	60.06	3.82	1.91	10500	13200
SHS 40×40×4 HR1	1/2 Span	39.98	39.79	3.85	2.19	5600	7010
SHS 40×40×4 HR2	1/3 Span	39.78	39.93	3.90	2.16	5650	7090
SHS 40×40×3 HR1	1/2 Span	40.22	39.9	3.01	2.07	4780	5850
SHS 40×40×3 HR2	1/3 Span	39.91	40.21	3.02	2.07	4820	5890
RHS 60×40×4 CF1	1/2 Span	40.20	60.14	3.89	2.07	10600	13400
RHS 60×40×4 CF2	1/2 Span	40.08	60.15	3.87	2.07	10500	13300
SHS 40×40×4 CF1	1/2 Span	40.36	40.37	3.72	3.10	5550	6930
SHS 40×40×4 CF2	1/3 Span	40.36	40.43	3.71	3.10	5550	6930
SHS 40×40×3 CF1	1/2 Span	40.20	40.08	2.72	2.63	4420	5370
SHS 40×40×3 CF2	1/3 Span	40.14	40.12	2.76	2.63	4470	5340

Table 2: Measured material properties of continuous beam specimens [4].

Tensile test specimen	Position	E	f_y	f_u	ε_f
		N/mm^2	N/mm^2	N/mm^2	
RHS 60×40×4 HR	Flat	213800	468	554	0.37
RHS 60×40×4 CF	Flat	212000	400	452	0.21
RHS 60×40×4 CF	Corner	202400	480	570	0.15
SHS 40×40×4 HR	Flat	212300	496	572	0.34
SHS 40×40×4 CF	Flat	201600	410	430	0.38
SHS 40×40×4 CF	Corner	210900	479	507	0.17
SHS 40×40×3 HR	Flat	219600	504	581	0.36
SHS 40×40×3 CF	Flat	212900	451	502	0.24
SHS 40×40×3 CF	Corner	196700	534	589	0.16

Table 3: Comparison of the hot-rolled steel continuous beam test results with FE results using different local imperfection amplitudes.

Continuous beam specimen	$F_{u,FE}/F_{u,test}$			
	b/100	*b*/200	*b*/300	*b*/400
RHS 60×40×4 HR1	1.07	1.08	1.09	1.09
RHS 60×40×4 HR2	0.99	1.01	1.02	1.02
SHS 40×40×4 HR1	0.94	0.96	0.97	0.98
SHS 40×40×4 HR2	1.05	1.07	1.08	1.08
SHS 40×40×3 HR1	1.04	1.05	1.06	1.06
SHS 40×40×3 HR2	0.96	0.98	0.98	0.99
Mean	1.01	1.03	1.03	1.04
COV	0.052	0.050	0.047	0.045

Table 4: Comparison of the cold-formed steel continuous beam test results with FE results using different conditions for corner strength enhancement and local imperfection amplitudes.

Continuous beam specimen	$F_{u,FE}/F_{u,test}$											
	Corners only				Up to *t* beyond corner				Up to 2*t* beyond corner			
	b/100	*b*/200	*b*/300	*b*/400	*b*/100	*b*/200	*b*/300	*b*/400	*b*/100	*b*/200	*b*/300	*b*/400
RHS 60×40×4 CF1	0.90	0.90	0.90	0.90	0.94	0.94	0.95	0.95	0.99	0.99	0.99	0.99
RHS 60×40×4 CF2	0.89	0.89	0.89	0.89	0.94	0.94	0.94	0.94	0.98	0.98	0.98	0.98
SHS 40×40×4 CF1	0.90	0.90	0.90	0.90	0.93	0.93	0.93	0.93	0.96	0.96	0.96	0.96
SHS 40×40×4 CF2	0.94	0.95	0.95	0.96	0.97	0.98	0.98	0.98	1.00	1.01	1.01	1.01
SHS 40×40×3 CF1	0.88	0.88	0.88	0.88	0.92	0.92	0.92	0.92	0.95	0.95	0.95	0.95
SHS 40×40×3 CF2	0.94	0.96	0.97	0.97	0.98	0.99	1.00	1.00	1.00	1.02	1.02	1.03
Mean	0.91	0.91	0.92	0.92	0.95	0.95	0.95	0.95	0.98	0.98	0.99	0.99
COV	0.029	0.035	0.038	0.040	0.023	0.029	0.032	0.033	0.021	0.025	0.028	0.029

Table 5: Material parameters used in parametric studies for hot-rolled steel continuous beams.

Steel grade	E	f_y	f_u	ε_u
	N/mm^2	N/mm^2	N/mm^2	%
S355	210000	355	490	16.53
S460	210000	460	540	8.89

Table 6: Material parameters used in parametric studies for cold-formed steel continuous beams.

Steel grade	Position	E	f_y	f_u	ε_u	n	m
		N/mm^2	N/mm^2	N/mm^2	%		
S355	Flat	203000	355	442	11.81	7.6	3.8
	Corner	203000	444	523	9.12	7.0	4.2
S460	Flat	203000	460	538	8.74	7.6	3.8
	Corner	203000	575	647	6.65	7.0	4.2

Table 7: Assessment of design methods for hot-rolled steel SHS and RHS continuous beams.

	Class 1 No. of FE (test) data: 1045 (6)			Class 2 and 3 No. of FE (test) data: 300 (0)		Cross-sections with $\overline{\lambda}_p \leq 0.6$ No. of FE (test) data: 1180 (6)		
	$F_{u,FE(test)}/F_{u,EC3}$	$F_{u,FE(test)}/F_{u,csm}$		$F_{u,FE(test)}/F_{u,EC3}$	$F_{u,FE(test)}/F_{u,csm}$	$F_{u,FE(test)}/F_{u,EC3}$	$F_{u,FE(test)}/F_{u,csm}$	
		$\varepsilon_{csm}/\varepsilon_y \leq 15$	$\varepsilon_{csm}/\varepsilon_y \leq 25$				$\varepsilon_{csm}/\varepsilon_y \leq 15$	$\varepsilon_{csm}/\varepsilon_y \leq 25$
Mean	1.18	1.18	1.14	1.27	1.22	1.18	1.17	1.13
COV	0.11	0.09	0.06	0.14	0.14	0.11	0.09	0.05

Table 8: Assessment of design methods for cold-formed steel SHS and RHS continuous beams.

	Class 1 No. of FE (test): 1045 (6)		Class 2 and 3 No. of FE (test): 300 (0)		Cross-sections with $\overline{\lambda}_p \leq 0.6$ No. of FE (test): 1147 (6)	
	$F_{u,FE(test)}/F_{u,EC3}$	$F_{u,FE(test)}/F_{u,csm}$	$F_{u,FE(test)}/F_{u,EC3}$	$F_{u,FE(test)}/F_{u,csm}$	$F_{u,FE(test)}/F_{u,EC3}$	$F_{u,FE(test)}/F_{u,csm}$
Mean	1.22	1.16	1.34	1.33	1.23	1.17
COV	0.06	0.03	0.15	0.14	0.07	0.03

Table 9: Summary of coefficients C_i for CSM material models.

Material	CSM material model	C_1	C_2	C_3	C_4
Hot-rolled carbon steel	Stages 1-3 of quad-linear model (Fig. 8)	Eq. (10)	Eq. (11)	0.60	0.00
Cold-formed carbon steel		0.40	0.45	0.60	0.00
Austenitic and duplex stainless steel	Elastic, linear hardening model (Fig. 9)	0.10	0.16	1.00	0.00
Ferritic stainless steel		0.40	0.45	0.60	0.00
Aluminium		0.50	0.50	0.13	0.06

Table 10: Summary of reliability analysis results for EC3 and the proposed CSM for hot-rolled and cold-formed steel SHS and RHS continuous beams.

Production route	Design approach	No. of FE (test) data	$k_{d,n}$	b	V_δ	V_r	γ_{M0}
Hot-rolled steel	EC3	1045 (6)	3.10	1.18	0.10	0.12	1.05
	CSM ($\varepsilon_{csm}/\varepsilon_y \leq 15$)	1180 (6)	3.10	1.17	0.09	0.11	1.02
	CSM ($\varepsilon_{csm}/\varepsilon_y \leq 25$)	1180 (6)	3.10	1.11	0.05	0.08	0.99
Cold-formed steel	EC3	1045 (6)	3.10	1.22	0.06	0.08	0.91
	CSM ($\varepsilon_{csm}/\varepsilon_y \leq 15$)	1147 (6)	3.10	1.17	0.03	0.07	0.90

Figures:

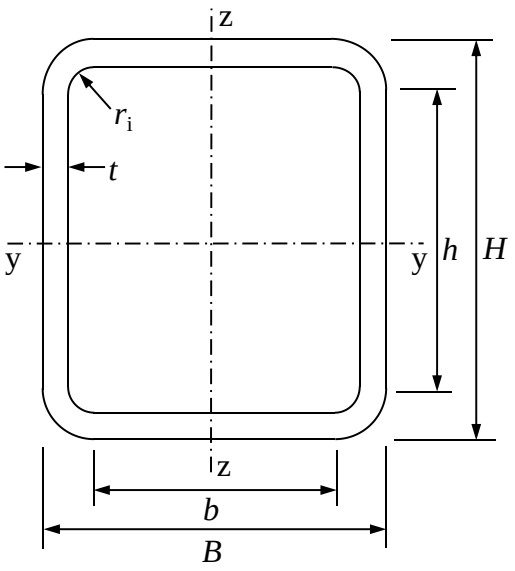

Fig. 1. Definition of symbols for SHS and RHS.

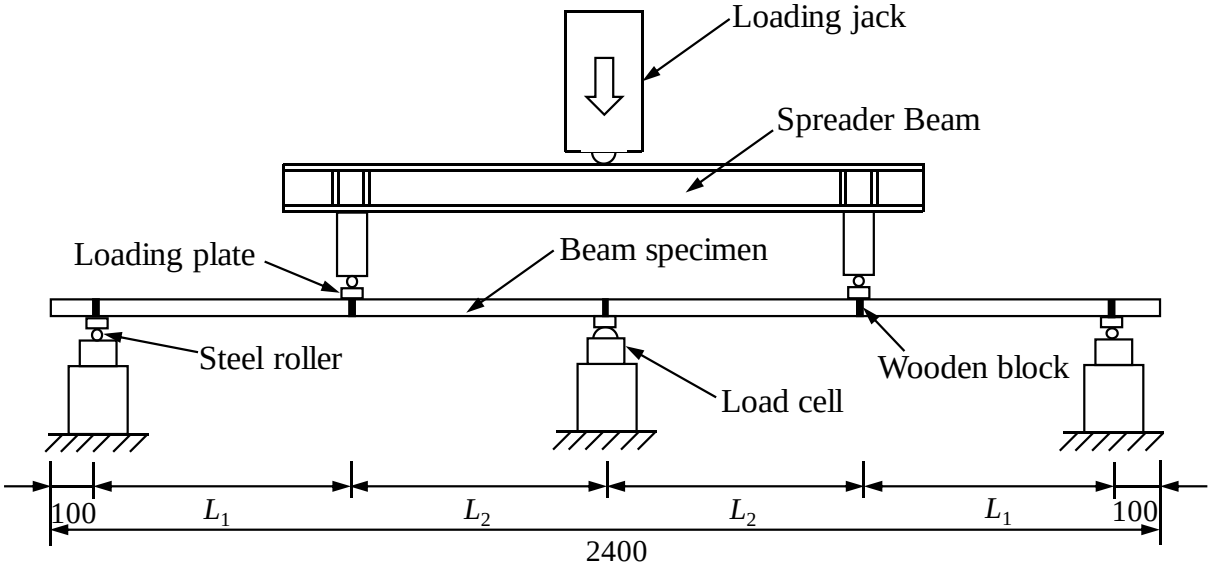

Fig. 2. Schematic diagram of the continuous beam test setup (dimensions in mm).

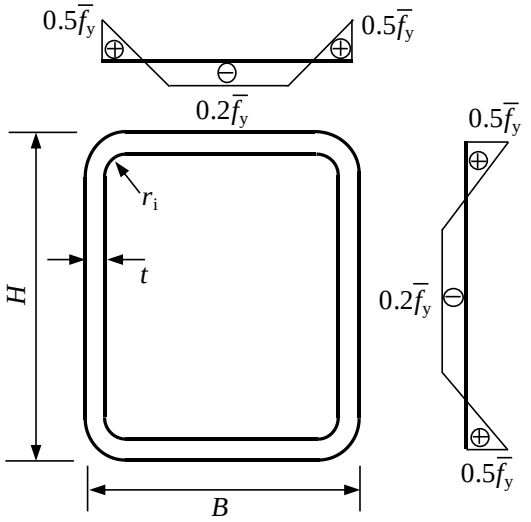

(a) Residual stress pattern recommended in ECCS [23]

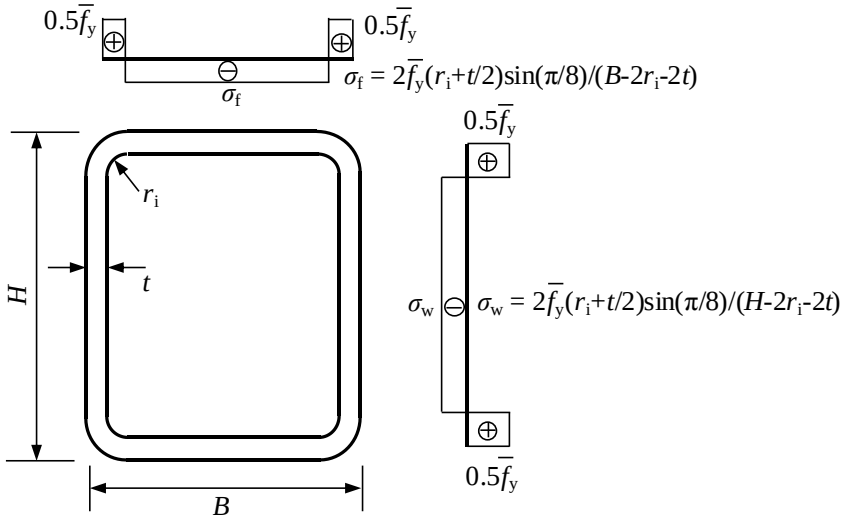

(b) Simplified residual stress pattern [8]

Fig. 3. Membrane residual stress patterns for hot-rolled steel SHS/RHS.

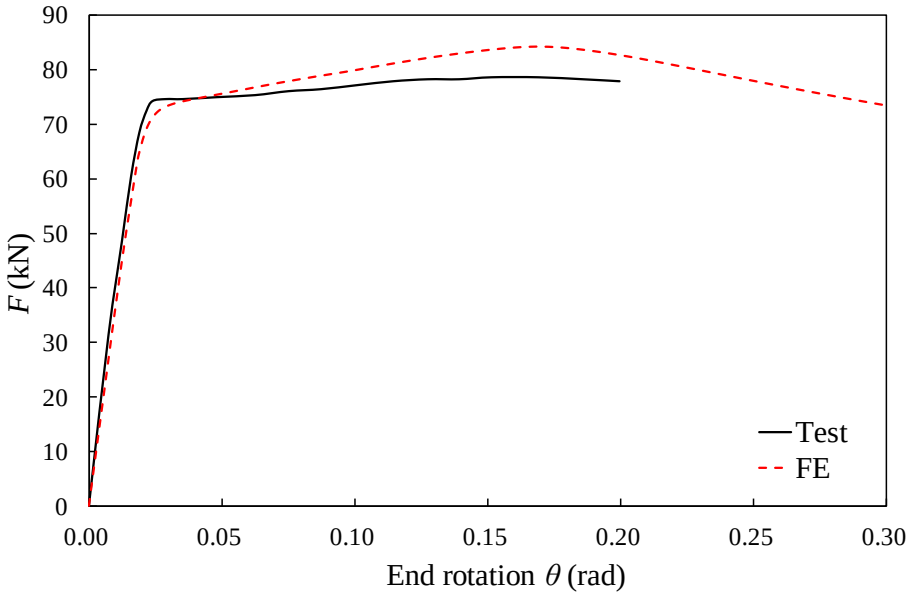

Fig. 4. Experimental and numerical load-end rotation curves for specimen RHS 60×40×4 HR1 tested in [4].

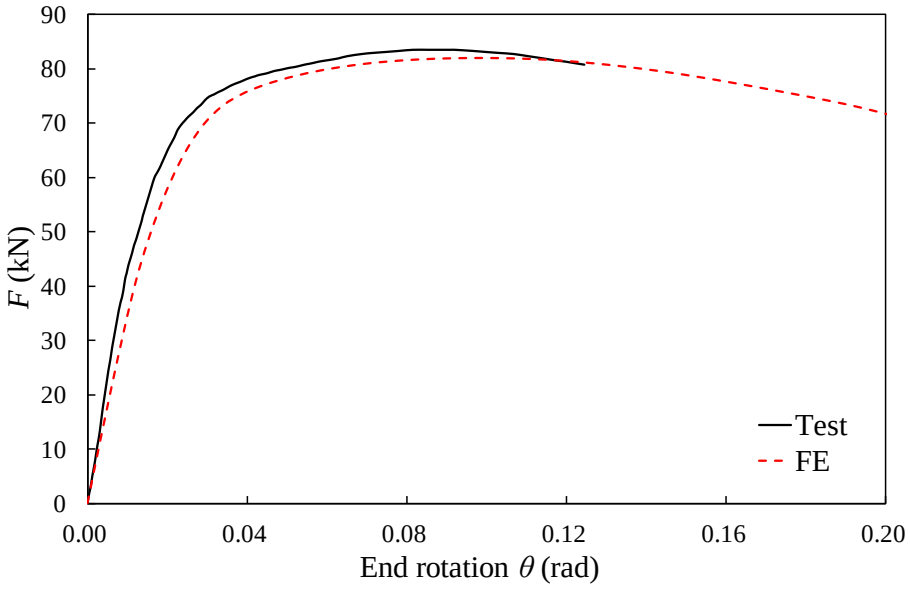

Fig. 5. Experimental and numerical load-end rotation curves for specimen RHS 60×40×4 CF1 tested in [4].

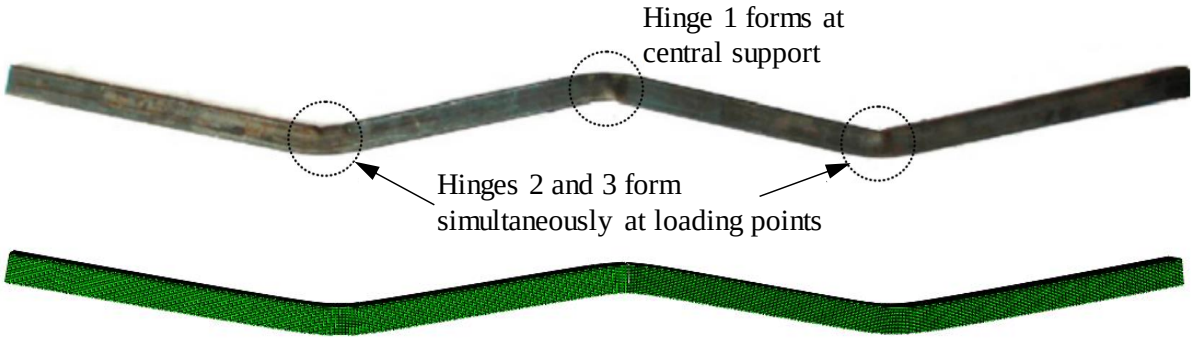

Fig. 6. Experimental and FE failure modes of two-span continuous beam specimen RHS 60×40×4 HR1 [4].

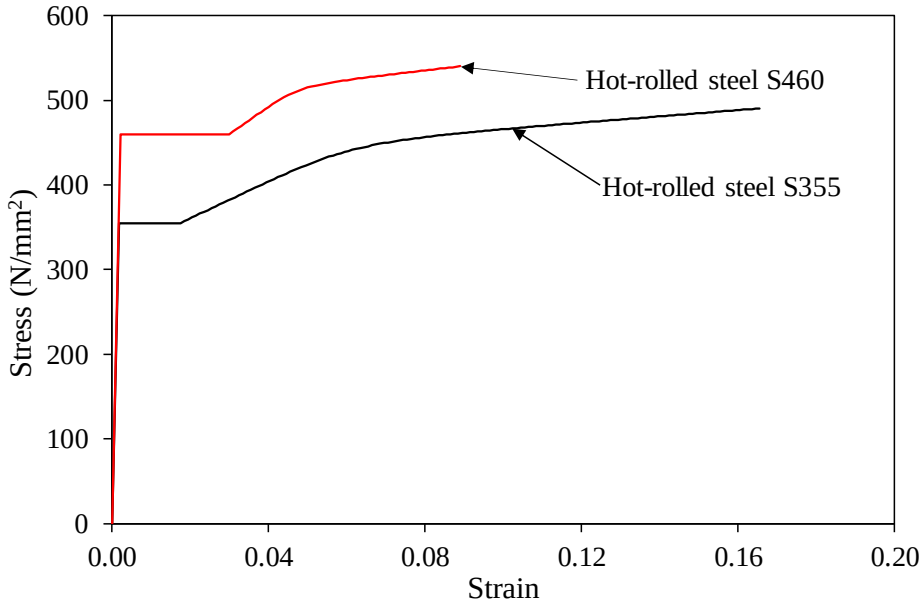

Fig. 7. Adopted stress-strain curves for parametric studies of hot-rolled steel sections [2].

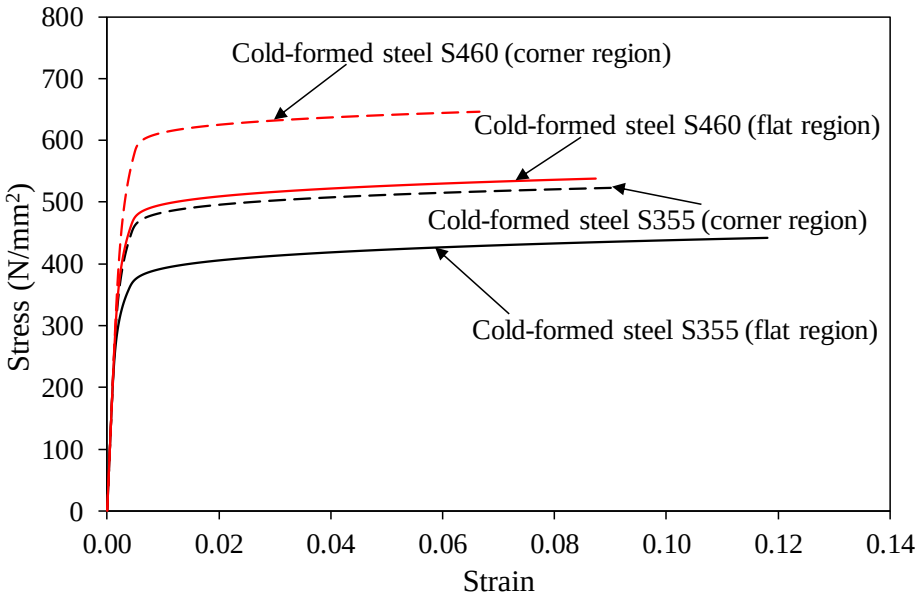

Fig. 8. Adopted stress-strain curves for parametric studies of cold-formed steel sections [3].

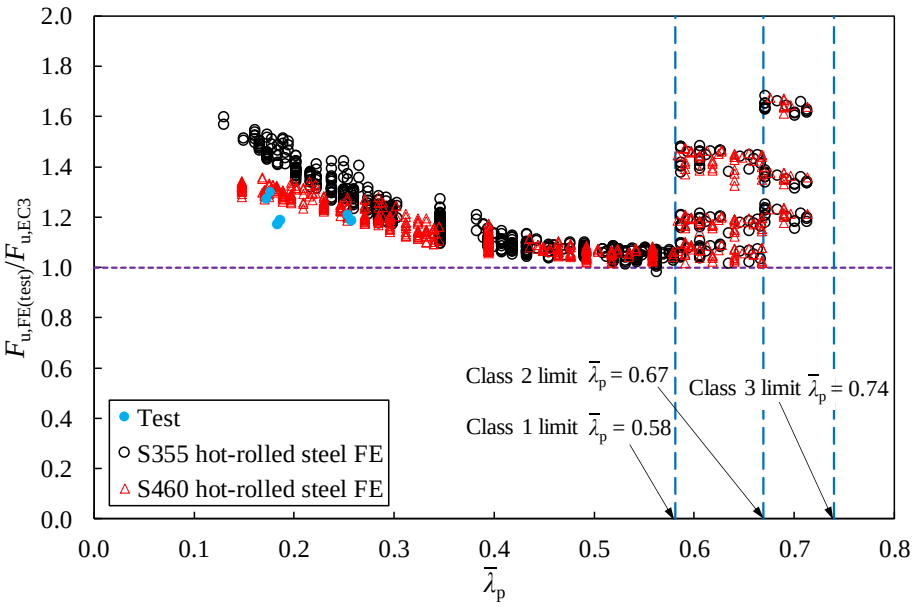

Fig. 9. Comparison of test and FE results with predicted ultimate loads from EN 1993-1-1 for hot-rolled steel SHS and RHS continuous beams.

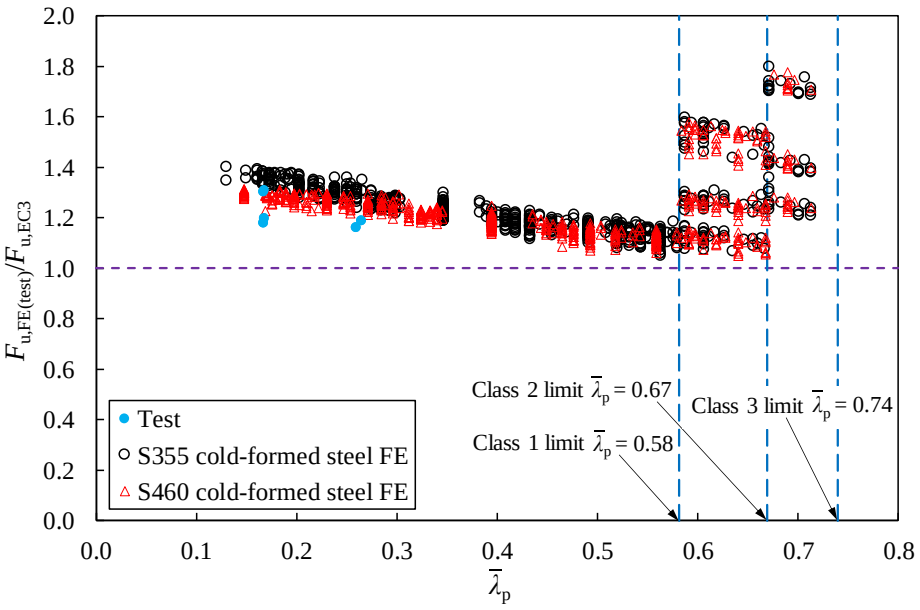

Fig. 10. Comparison of test and FE results with predicted ultimate loads from EN 1993-1-1 for cold-formed steel SHS and RHS continuous beams.

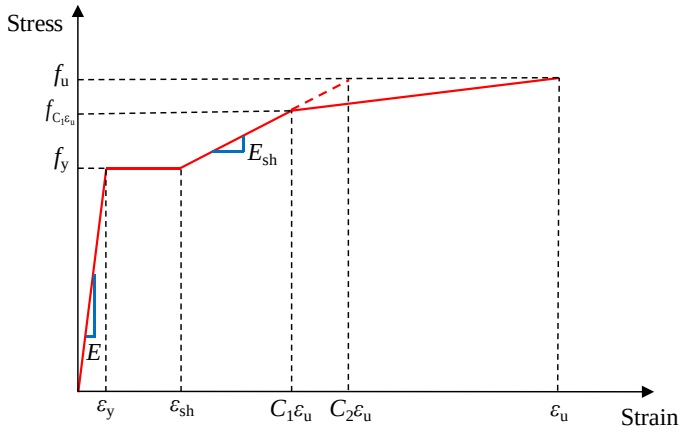

Fig. 11. Quad-linear material model for hot-rolled carbon steels [2].

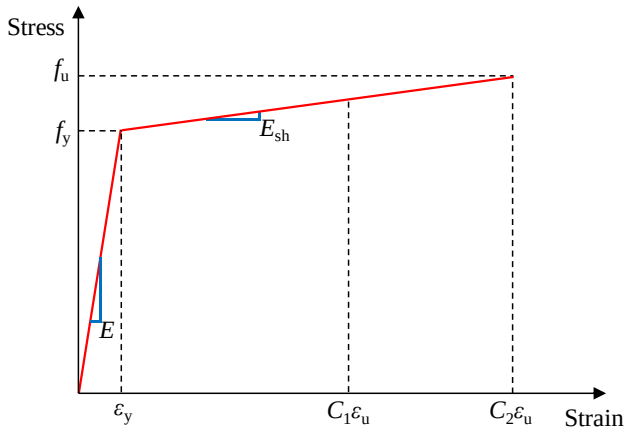

Fig. 12. Elastic, linear hardening material model for cold-formed carbon steels [12].

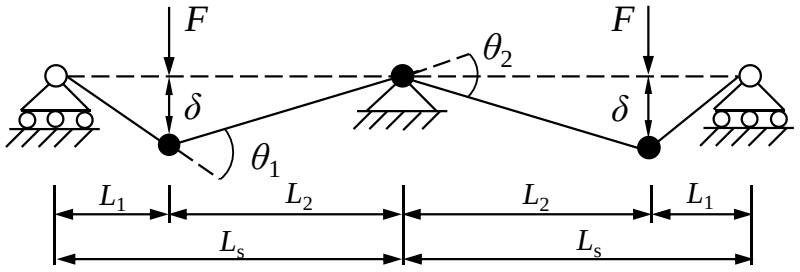

Fig. 13. Plastic collapse mechanism for two-span continuous beams.

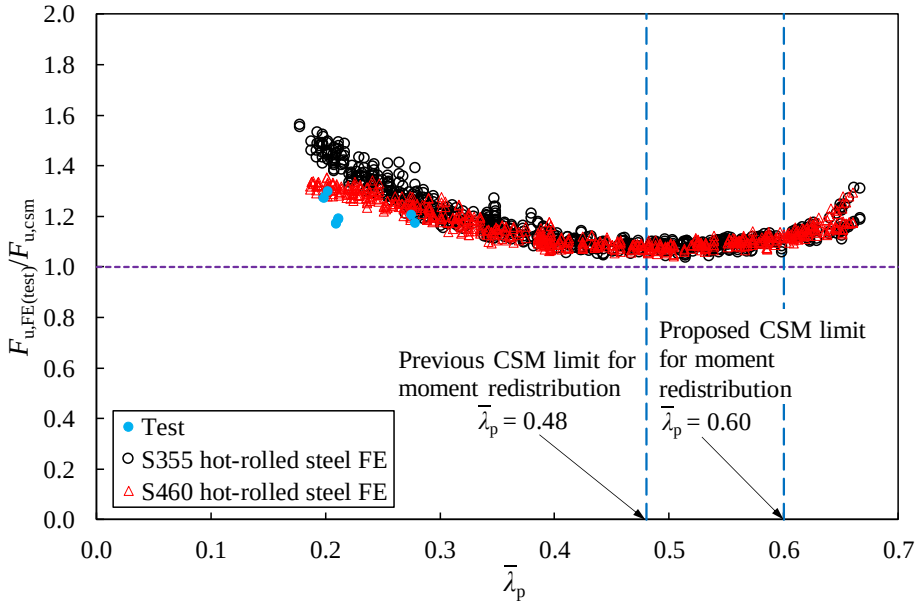

Fig. 14. Comparison of test and FE results with predicted ultimate loads from the CSM ($\varepsilon_{csm}/\varepsilon_y \leq 15$) for hot-rolled steel SHS and RHS continuous beams.

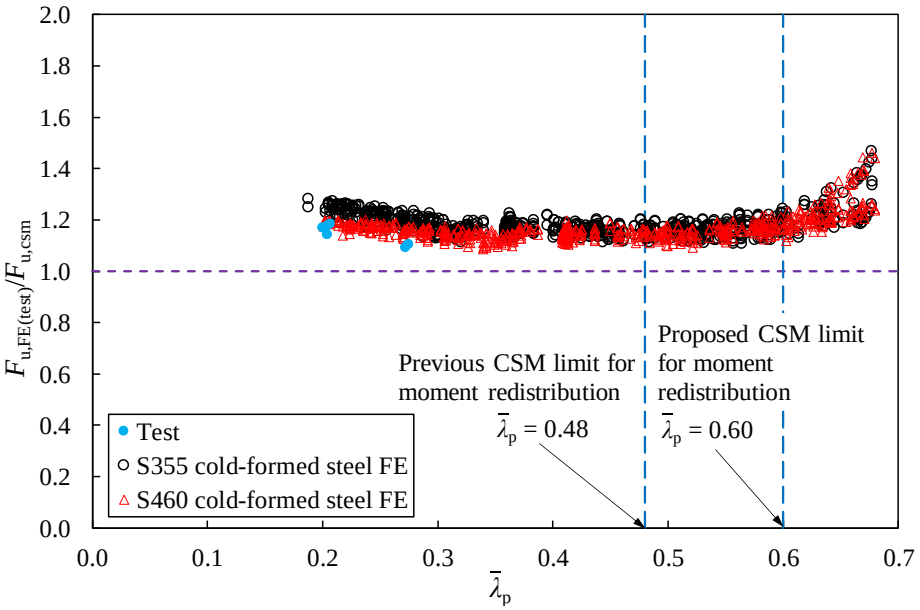

Fig. 15. Comparison of test and FE results with predicted ultimate loads from the CSM for cold-formed steel SHS and RHS continuous beams.

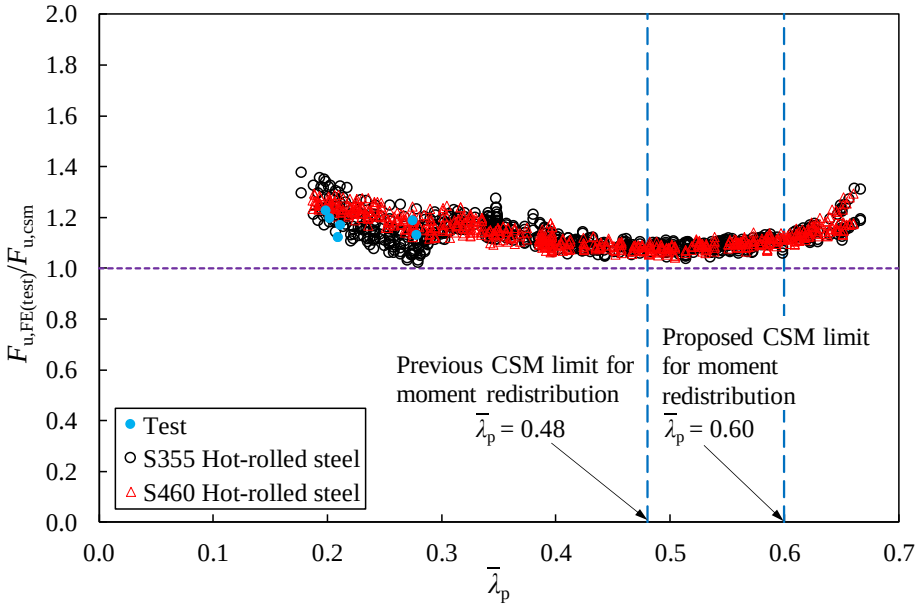

Fig. 16. Comparison of test and FE results with predicted ultimate loads from the CSM ($\varepsilon_{csm}/\varepsilon_y \leq 25$) for hot-rolled steel SHS and RHS continuous beams.